Brownian motion of ellipsoidal particles on a granular magnetic bath

C. Tapia-Ignacio [1] R. E. Moctezuma,[2] F. Donado,[1] and Eric R. Weeks [3,*]

[1]*Instituto de Ciencias Básicas e Ingeniería, Universidad Autónoma del Estado de Hidalgo, Mineral de la Reforma 42184, Hidalgo, México*
[2]*CONACYT-Instituto de Física "Manuel Sandoval Vallarta", Universidad Autónoma de San Luis Potosí, Alvaro Obregón 64,
78000 San Luis Potosí, S.L.P., México*
[3]*Physics Department, Emory University, Atlanta, Georgia 30322, USA*

We study the Brownian motion of ellipsoidal particles lying on an agitated granular bath composed of magnetic particles. We quantify the mobility of different floating ellipsoidal particles using the mean-square displacement and the mean-square angular displacement, and relate the diffusion coefficients to the bath particle motion. In terms of the particle major radius R, we find the translational diffusion coefficient scales roughly as $1/R^2$ and the rotational diffusion coefficient scales as roughly $1/R^4$; this is consistent with the assumption that diffusion arises from random kicks of the bath particles underneath the floating particle. By varying the magnetic forcing, the bath particles' diffusivity changes by a factor of ten; over this range, the translational and rotational diffusion of the floating particles change by a factor of 50. However, the ratio of the two diffusion constants for the floating particles is forcing-independent. Unusual aspects of the floating particle motion include non-Gaussian statistics for their displacements.

I. INTRODUCTION

Brownian motion (diffusion) occurs in a wide variety of processes in nature. While initially observed in regular liquids, its theory has been applied not only in physics, but in biology, chemistry, and even economics. In macroscopic granular systems, external forcing can effectively "thermalize" the system and result in diffusive motion [1–7]. In super-cooled liquids, diffusion slows greatly, but with rotational diffusion of nonspherical probes slowing even more than translational diffusion [8–12]. Some granular experiments [5,13–15] and simulations [16,17] showed that granular systems can exhibit glassy behavior under some conditions, with diffusive motion greatly slowed. However, rotational diffusion has not been studied in these granular experiments.

In this paper, we study the translational and rotational behavior of floating ellipsoidal particles on a magnetic granular bath, and examine the influence of the bath particle intensity on the motion of the floating particles. By varying the forcing applied to the magnetic bath particles, we can vary the diffusivity of the floating particles by nearly two orders of magnitude. For low magnetic forcing, the bath particles exhibit subdiffusive behavior somewhat like a supercooled fluid. Our overall goal is to understand the behavior of the floating particles as subjected to this particular form of effective "thermal" forcing as we vary the motion of the bath particles; essentially, to add our previously described system [5,18,19] to the above mentioned examples of granular "thermal baths" [1–4]. Across the range of bath particle conditions, we find that the floating particles always have rotational diffusion and translational diffusion coupled, that is, their ratio is constant.

While the coupling of the diffusion constants is to be expected for particles in a "normal" fluid, we find other unusual aspects of the floating particle motion such as non-Gaussian statistics. Evidence from examining different sizes of floating particles suggests that the diffusive motion can be understood as due to temporally periodic, randomly oriented kicks from the bath particles.

II. EXPERIMENTAL SETUP

The experimental configuration consists of a flat particle floating on a forced granular medium; see Fig. 1. This granular medium is composed of a 2D ensemble of stainless steel spherical particles of diameter 1 mm, mass 4.2 mg, and area fraction 0.23. The system is placed in a time-dependent magnetic field. The steel particles have been previously magnetized so that they possess a permanent magnetic dipole. The magnetic field is generated by a pair of Helmholtz coils fed by a power amplifier driven such that the magnetic field is $B_c + B_o \sin 2\pi f t$, oriented vertically. The oscillatory component causes the particles to move randomly: each steel particle tries to align its magnetic dipole moment with the instantaneous field (pointing up or down), causing the particle to rotate in a random direction to implement the reorientation. When the field reverses, the particle tries to reorient, subject to the rotational inertia it already possesses. The result is that the steel particle motion is quite random and plays the role of a thermal bath. The bath particles roll and slide, but always remain in contact with the surface; bouncing is not observed.

Decreasing B_o toward B_c results in an effectively "cooler" granular bath, as the particles spend less time during the cycle needing to reorient their dipoles. The constant magnetic field component B_c ensures that the particles spend more time with vertically oriented magnetic dipoles, and these aligned dipoles
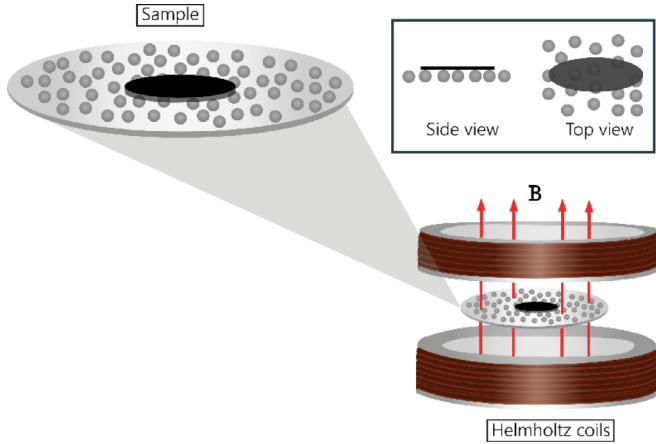
———————
*erweeks@emory.edu

FIG. 1. The experimental setup consists of magnetic particles in a horizontal container (diameter 132 mm) in the middle of Helmholtz coils (inner diameter 152 mm, outer diameter 179 mm). A sinusoidal signal fed into a power amplifier produces an alternating magnetic field. The spherical bath particles have permanent magnetic dipoles so the changing field causes the particles to roll on the surface in random directions. A flat particle "floats" on the bath particles and moves due to the random kicks it receives from the underlying bath particles.
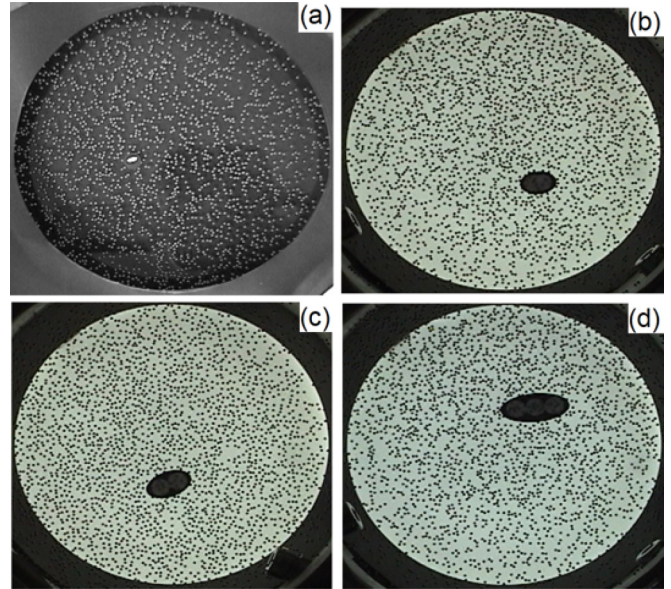

FIG. 2. Images showing floating particles with aspect ratio (a) $\alpha = 1.00$, (b) $\alpha = 1.44$, (c) $\alpha = 1.48$, and (d) $\alpha = 2.20$. The bath particles are the smaller spheres. Note that the image in (a) is viewed with reflected light, while the other are viewed with transmitted light, leading to the different appearance of panel (a) from the other panels. The circular particle in panel (a) has a white ellipse drawn on it to facilitate rotational tracking of this otherwise circularly symmetric particle.

repel each other, thus frustrating the formation of permanent magnetic clusters which are observed in the absence of a constant magnetic field component [20,21]. Although this system is highly dissipative, it reaches a stationary state which fits the necessary conditions to be considered as an Ornstein-Uhlenbeck stochastic process [18]. The dynamics of a system similar to these bath particles has already been studied, and it has been demonstrated that for certain conditions the magnetic field is proportional to an effective temperature [19].

For all experiments, we use $B_c = 33$ G for the constant component. The intensity of the bath particle motion is varied with the magnitude of the oscillating magnetic field: $B_o = 66$, 60, 54, 48, 42, 36, and 30 G, all of them with a frequency of $f = 10$ Hz. In this system, for high intensities of the field, the bath particles show the dynamics similar to that of a Brownian gas, and the velocity distributions are Maxwell-Boltzmann distributions [19]. For low intensities, the motion of the particles decreases, showing freezinglike effects resembling the dynamics near the glass transition [5]. For the lowest amplitude we consider ($B_o = 30$ G), we have $B_o < B_c$ and thus the imposed magnetic field never changes direction; the magnetic dipoles do not need to rotate. Nonetheless, the particles are observed to still rotate and move, albeit slowly. This may be due to two possibilities. First, the Earth's magnetic field (measured to be 0.6 G) is at an angle to the imposed vertical field, and that slight off-vertical component to the field perhaps causes some particle rotation at the times when the absolute magnitude of the imposed magnetic field is the smallest. Second, the oscillating magnetic field likely gives a time varying component to the particles' magnetic dipoles, causing a time varying repulsive interaction and thus causing the particles to move. Evidence for this second mechanism is that at lower area fractions, the particles are no longer observed to move other than small vibrations. At the area

fraction used in this work ($\phi = 0.23$), when B_o is less than 30 G, the spatial distribution of the bath particles becomes inhomogeneous during the course of the experiment, thus preventing us from conducting long duration experiments at low bath particle motion.

We conduct two series of experiments. One is a study of the size dependence of the floating particle motion, and the other is a study of the forcing dependence of the floating particle motion. These two series of experiments use different bath particles. By chance, the bath particles for the size dependence experiments are less magnetized than the bath particles for the forcing dependence. For this reason, while we report the amplitude of the oscillatory magnetic field B_o for the results discussed in the next section, a more useful characterization is the length scale L defined by the bath particle mean-square displacement: $L^2 = \langle \Delta r^2 \rangle (\Delta t = 0.1 \text{ s})$. The timescale $\Delta t = 0.1$ s is chosen to match the forcing frequency; further justification for this choice is presented below.

We use floating particles with aspect ratios ranging from $\alpha = 1.00$ to $\alpha = 2.20$, as shown in Fig. 2. Further details of these particles are listed in Table I. The floating particles are nonmagnetic, and do not interact with the magnetic field. Rather, they sit atop the magnetic bath particles, and move due to the random kicks of the bath particles. The floating particles experience frictional forces from the bath particles, and also the bath particles occasionally collide with the edges of the floating particles. The floating particles are sufficiently stiff that they remain flat and essentially horizontal. In particular, we avoid using smaller floating particles which would tilt out of plane. Observations of the bath particles underneath

TABLE I. Details of the floating particles, including semimajor diameter and semiminor diameter. The particles are cut from paper with a thickness of 0.12 mm and an area density of 0.073 mg/mm².

Aspect ratio	$2r_{major}$	$2r_{minor}$	mass
1.00	6.4 mm	6.4 mm	2.2 mg
1.44	13.0 mm	9.0 mm	7.1 mg
1.48	17.0 mm	11.5 mm	10.4 mg
2.20	24.4 mm	11.1 mm	17.0 mg

the floating particles are possible, as the floating particles are semi-transparent; we find the bath particles underneath have a mean-square displacement roughly 80% the magnitude of the particles away from the floating particle. We observe that particles enter and exit the floating particle region constantly throughout the experiments.

For the size dependence experiments, we obtain one 3-min video for each floating particle. For the forcing dependence experiments, we obtain three series of 3-min videos for each floating particle and magnetic forcing amplitude. From each video we track the translational and rotational motion of the floating particle, along with the bath particle motion [22]. Our temporal resolution is 1/60 s, our spatial resolution is better than 0.07 mm (x and y position), and our angular resolution is better than 0.006 rad ($\approx 0.4°$). As is apparent from Fig. 2, the images are slightly compressed in the vertical direction, which is accounted for in the analysis (both in the translational calibration and the angular calibration). Even at the highest level of forcing, it is rare for the floating particle to move close to the container boundary within three minutes. We exclude movies where this occurs from the data analysis.

III. RESULTS

A. Size dependence

We first wish to understand the dependence of diffusion on the floating particle size. To do this, we use our largest forcing ($B_o = 66$ G) although with the less magnetized bath particles. The motion of the bath particles over a 0.1 s timescale is $L = \sqrt{\langle \Delta r^2 \rangle} = 1.6$ mm. In this situation, the bath particles are diffusive at timescales $\Delta t > 1$ s. We find that the floating particles are also diffusive, and so we study how the diffusion coefficient depends on particle size. In a 3D Newtonian fluid, the rotational motion of ellipsoids follows $D_T \sim 1/r_{major}$, $D_R \sim 1/r_{major}^3$, in part because the two diffusion coefficients have different units [28–30]. In our experiments it is more precise to measure the floating particles' masses rather than their radii, so accordingly we plot D_T and D_R as functions of mass m in Fig. 3. We find roughly that $D_T \sim m^{-1}$ and $D_R \sim m^{-2}$, as shown by the superimposed lines in Fig. 3. As $m \sim$ area $\sim r^2$, this shows that the diffusivity behaves differently in our experiment than the 3D Brownian motion case, although the ratio D_T/D_R scales as $\sim r^2$ for our experiment as is also the case for 3D Brownian diffusion. Indeed, the ratio $mD_T/\rho D_R$ is plotted in Fig. 3(c) and within uncertainty appears independent of m; this uses the area density of the paper ($\rho = 0.073$ mg/mm²) to simplify the units. Within the uncertainty, this ratio is independent of the aspect ratio [mean ratio is 5.78 ± 1.29
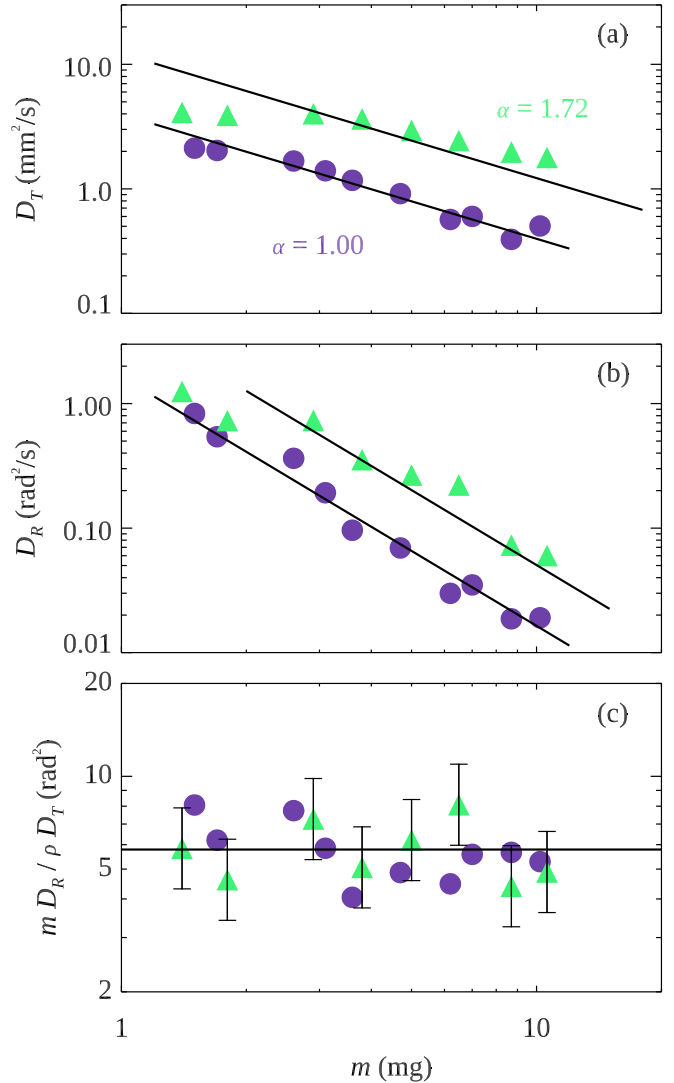

FIG. 3. (a) Translational diffusion coefficient D_T as a function of floating particle mass for ellipses (aspect ratio $\alpha = 1.72$) and circular particles ($\alpha = 1.00$) as labeled. The fit lines are constrained to follow $D_T \sim 1/m$. Unconstrained least-squares fits give power law exponents of -0.9 (circular particles) and -0.4 (ellipses). (b) Rotational diffusion constants D_R for the same particles. The fit lines are constrained to follow $D \sim 1/m^2$. Unconstrained least-squares fits give power law exponents of -2.1 (circular particles) and -1.5 (ellipses). The uncertainties of the diffusivity data in panels (a) and (b) are the symbol size. (c) Ratio $mD_R/\rho D_T$ as a function of mass m. The horizontal line shows the mean value for all data, 5.8 ± 1.3 rad² (mean $\pm$ standard deviation). The uncertainty of the ratio data is $\pm 35\%$, with representative error bars for the ellipse data.

for $\alpha = 1.00$, 5.80 ± 1.32 for $\alpha = 1.72$, (mean plus or minus standard deviation)].

The $1/r^2$ dependence of the translational diffusion coefficient is plausibly due to the random kicks of the tracer particles. As noted above, the bath particles have an area fraction $\phi = 0.23$. An elliptical floating particle with aspect ratio α and minor axis radius r will cover $N = \alpha \pi r^2 \phi$ bath particles on average. During one period of the oscillatory magnetic field ($\tau = 0.1$ s), each bath particle kicks the floating particle

in a random direction. Adding these kicks randomly, the net force should be proportional to $(\alpha \pi r^2 \phi)^{1/2} \sim r$. The mass of the particle is proportional to the area which is proportional to r^2, so the acceleration of the floating particle during τ is proportional to $1/r$. The displacement of the floating particle during that time is proportional to acceleration and thus $1/r$. Assuming that the bath particle motion is random each period, the Central Limit Theorem yields a diffusion coefficient $D_T = (\text{displacement})^2/2\tau \sim 1/r^2 \sim 1/m$, in agreement with the results of Fig. 3(a). The data show this argument is a bit simplistic, as it would predict that D_T does not depend on aspect ratio, whereas Fig. 3(a) shows that for the same mass, the elliptical particle has a larger translational diffusion constant (by a factor of 3.1).

A similar line of reasoning for the rotational motion leads to $D_R \sim 1/r^4$. A bath particle exerts a torque proportional to r, and assuming again the N torques add randomly, the net torque should be proportional to r^2. The moment of inertia for a circular disk is $I = mr^2/2 \sim r^4$, so the angular acceleration and thus angular displacement during one oscillation period scale as $1/r^2$. This leads to $D_R \sim 1/r^4 \sim 1/m^2$, the relationship indicated by the solid lines in Fig. 3(b). This works very well for the circular floating particles (circle symbols in the figure), and less well for the elliptical floating particles (triangle symbols). The deviations suggest that the interaction between the bath particles and the floating particles may be more complex than we assume here. For D_R, we find the ellipses diffuse a factor of 3.1 times faster than the circles for equivalent m, the same factor as for D_T.

B. Varying forcing intensity

We now turn to the experiments varying the forcing intensity. As noted in Sec. II, these experiments are done with bath particles that are more strongly magnetized and which thus can be agitated quite strongly by the oscillatory magnetic field. To characterize the motion of the bath particles, we calculate the mean-square displacement (MSD) for each magnetic field amplitude we consider. The results are shown in Fig. 4. It is interesting to note that for all of the data, at short Δt, the MSD of the bath particles is superdiffusive with $\langle \Delta r^2 \rangle \sim \Delta t^{1.7}$. This implies that over a short timescale particles are more likely to move in straight lines, rather than being purely diffusive random walks [23]. At high magnetic field intensities, the motion of the bath particles is diffusive (top curves of Fig. 4). As the magnetic field intensity decreases, bath particle motion is slower. At the lowest forcing, the MSD has a short subdiffusive bend around $0.1 < \Delta t < 0.3$ s (bottom curve of Fig. 4). Even at longer timescales ($\Delta t > 1$ s) it does not quite achieve diffusive behavior, but rather follows $\langle \Delta r^2 \rangle \sim \Delta t^{0.8}$. This resembles a supercooled fluid close to the glass transition [24–27].

We likewise consider the floating particle motion, which has both translational and rotational components. Example translational and rotational trajectories of a floating particle with aspect ratio $\alpha = 2.20$ for a high and a low excitation case are shown in Fig. 5. Both the rotational orientation and the position in x show a greater variation for higher excitations than for the lower ones. The full trajectories
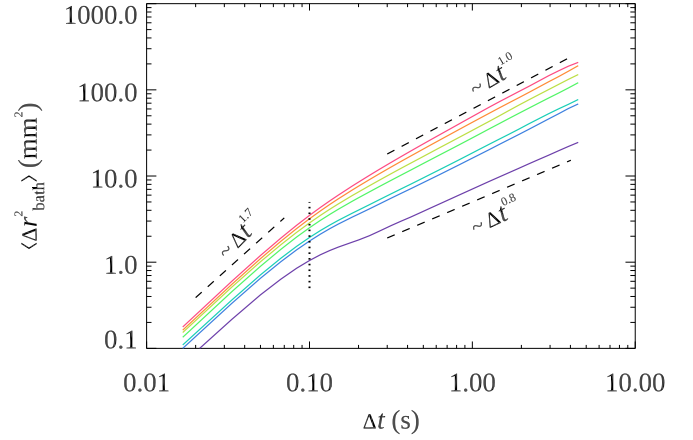

FIG. 4. Mean-square displacement $\langle \Delta r^2_{\text{bath}} \rangle$ for the bath particles. The vertical dotted line indicates the timescale (0.1 s) corresponding to the period of the magnetic forcing. The intersection of the data with this vertical line sets the length scale L through $L^2 = \langle \Delta r^2 \rangle (\Delta t = 0.1 \text{ s})$. The dashed lines indicate power law growth with the exponents as labeled. The lowest forcing (30 G) of the bath particles corresponds to the purple curve at the bottom and increases up to 66 G (red curve at the top).

for high excitations expand noticeably over a larger area compared with the trajectories at low excitations (insets of Fig. 5).

Figure 6 shows the MSD $\langle \Delta r^2 \rangle$ and the mean-square angular displacement (MSAD) $\langle \Delta \theta^2 \rangle$ for the floating particle with aspect ratio $\alpha = 2.20$. The vertical dotted line corresponds to the period of the magnetic forcing, and coincides with a crossover region from short timescale behavior to long timescale behavior. In all cases there is diffusive behavior at large timescales for both MSD and MSAD, regardless of the excitation of the bath. This result is interesting, since it
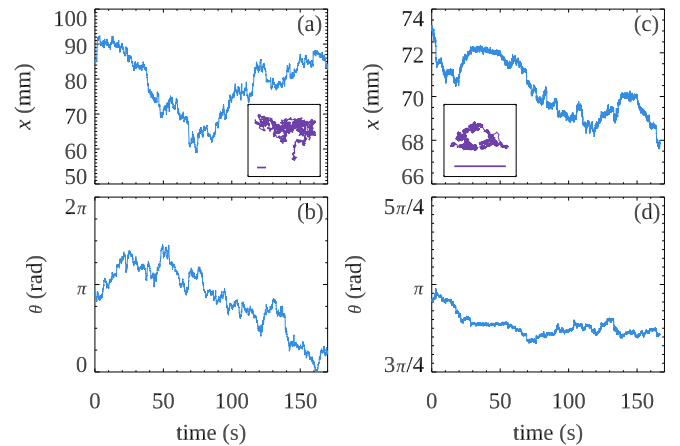

FIG. 5. Trajectories for the floating particle with aspect ratio $\alpha = 2.20$ for a high excitation case with $L = 1.68$ mm (a, b) and a low excitation case with $L = 0.92$ mm (c, d). Panels (a, c) show the x position as a function of time. The insets show the full trajectory in x and y with scale bars of length 5 mm. Panels (b, d) show the corresponding angular orientation as a function of time. Note the vertical scales are significantly reduced in panels (c, d) as compared to panels (a, b).
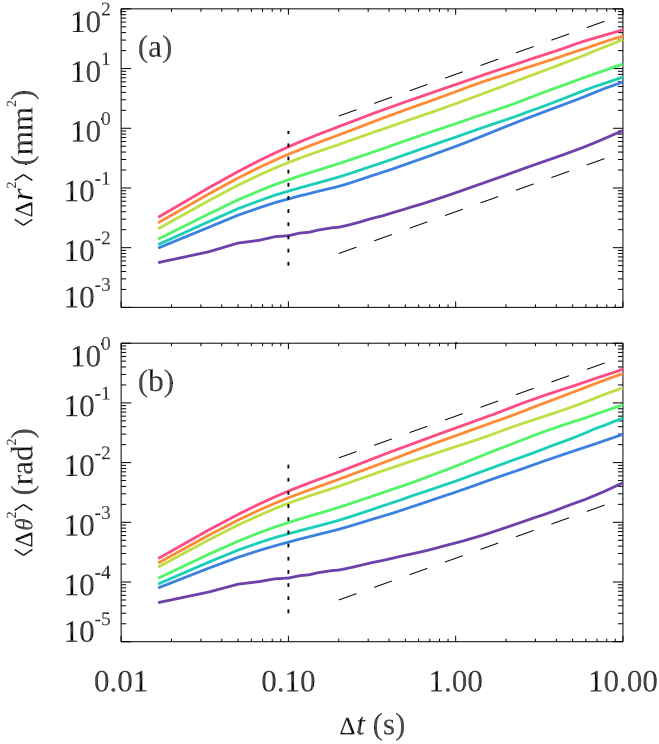
FIG. 6. (a) Mean-square displacement $\langle \Delta r^2 \rangle$ for the longest floating particle ($\alpha = 2.20$). The color of each curve relates to the intensity of the bath particle motion; see text for details. The vertical dotted line indicates the timescale (0.1 s) corresponding to the period of the magnetic forcing. The dashed lines indicate linear dependence $\langle \Delta r^2 \rangle \sim \Delta t$. (b) Mean-square angular displacement $\langle \Delta \theta^2 \rangle$. The colors are the same as in panel (a).

FIG. 7. (a) Translational diffusion coefficients D_T as a function of the forcing L. The different symbols are for different aspect ratio floating particles as indicated. (b) Rotational diffusion coefficients D_R as a function of the forcing L. The symbols are the same as in panel (a). For both panels, all fit lines have a constant slope: $\ln(D) \sim L/L_1$ with $L_1 = 0.23$ mm. The uncertainty in D is the symbol size.

indicates that, although the bath particles goes from diffusive to subdiffusive as we decrease the magnetic forcing (Fig. 4), the floating particles maintain their diffusive behavior. Intriguingly, the bath particle MSDs all have a constant initial power law growth (Fig. 4, constant initial slope on the log-log plot), whereas the floating particle MSDs exhibit an initial slope dependent on the forcing. Thus, within the timescales $\Delta t < 0.1$ s (the forcing period), the coupling between the bath particles and floating particles is nontrivial. The $\Delta t \to \infty$ behavior is also interesting: for the bath particles, the log-log slope of the MSD changes with the magnetic forcing intensity, whereas for the floating particles their behavior is always diffusive at long timescales (slope = 1 on the log-log plot).

The differing behavior at long timescales between the bath particles and the floating particles suggests that the direct influence of the bath is only at shorter timescales; that the diffusive behavior of the floating particles is emergent from the random steps that occur for each cycle of the oscillatory magnetic forcing. To investigate this, we fit the $\Delta t \to \infty$ portion of the floating particle MSD and MSAD curves to determine the diffusion coefficients through $\langle \Delta r^2 \rangle = 4 D_T \Delta t$, $\langle \Delta \theta^2 \rangle = 2 D_R \Delta t$. We then examine the dependence of the measured diffusion coefficients on various quantities related to the bath particles. In particular we use the bath particle motions (quantified by the MSD) using a natural choice for the timescale, $\Delta t = 0.1$ s (the period of the magnetic forcing). We
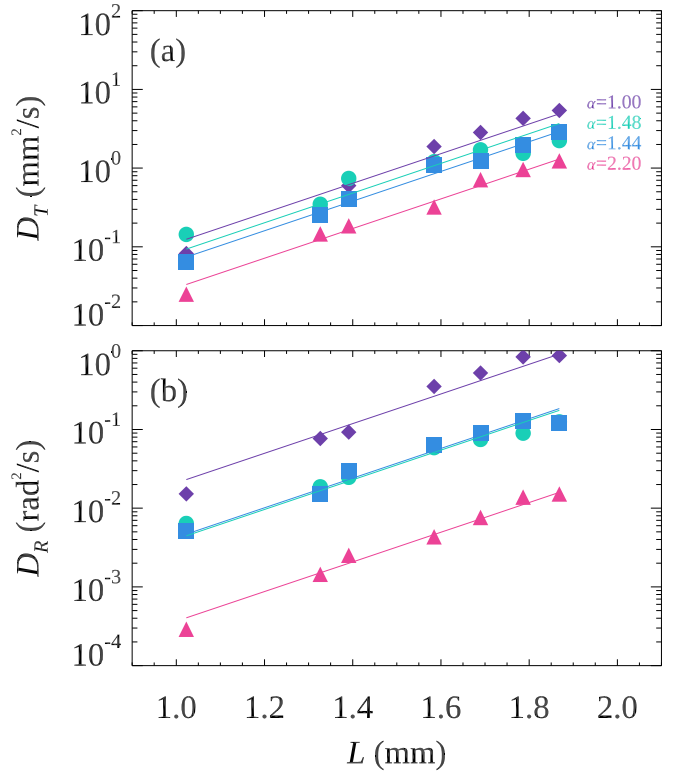
define a length scale $L = \sqrt{\langle \Delta r^2_{\text{bath}} \rangle}$ using displacements over this timescale. Figure 7 shows a linear relationship between L and the logarithms of all of the diffusion coefficients. This relationship, $\ln(D) \sim L/L_1$, holds for all our results with a common length scale $L_1 = 0.23$ mm; this is clear from the least-square fit lines in Fig. 7 where the fit is constrained to have a common slope and differing intercepts. Defining L with a different Δt gives results that have a larger least-square fit error, reinforcing our choice to use $\Delta t = 0.1$ s.

We note that fitting the diffusion coefficients to $\ln(D) \sim L^2/L_2^2$ works nearly as well, with $L_2 = 0.82$ mm. The least-square error is slightly larger, but the overall appearance is similar to the results shown in Fig. 7. The two fitting constants L_1 and L_2 are both similar in order of magnitude to the bath particle radius 0.5 mm. The dependence of $\ln(D)$ on L or L^2 suggests something like an activated process, although it is not apparent why this would be the case.

We next wish to compare D_T to D_R. As noted above, for diffusion in three dimensions, one expects $D_R/D_T \sim 1/r_{\text{major}}^2$. For our particular particles Fig. 3(c) shows that $m D_R / \rho D_T = A D_R / D_T$ collapses the data for different sizes of floating particles in terms of floating particle mass m, floating particle area density ρ, and area of floating particle A. Accordingly, we consider this nondimensional ratio plotted as a function of L in Fig. 8. Given that D_T and D_R have the same functional dependence on L (Fig. 7), it must be true that their ratio is
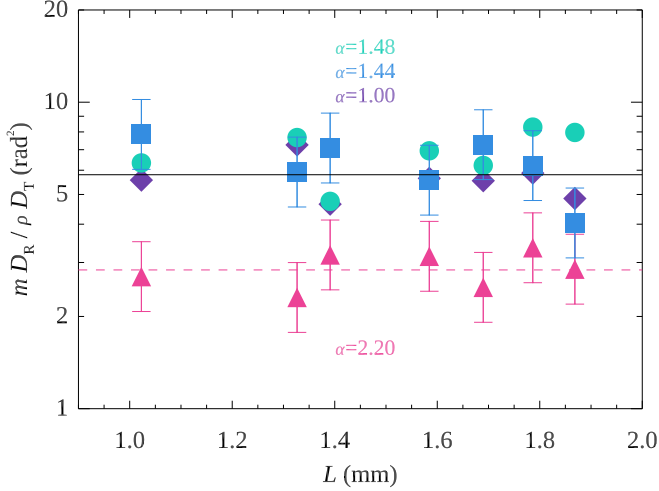
FIG. 8. The ratio of diffusion coefficients for floating particles with aspect ratios as indicated, as a function of the forcing intensity L. The ratio is nondimensionalized by multiplying by m/ρ, which is the area of the floating particle. Representative error bars are shown for the $\alpha = 1.44, 2.20$ data sets; the uncertainties of the other data sets are identical. The solid horizontal line indicates 5.8 rad^2 [taken from Fig. 3(c)] and the dashed horizontal line indicates 2.8 rad^2 (the mean value for the $\alpha = 2.20$ data). Taken individually, the mean values for $\alpha = 1.00, 1.44, 1.48$ are 5.6, 6.2, 6.8 rad^2.

a constant, as Fig. 8 shows (within the uncertainty). For $\alpha = 1.00$, 1.44, and 1.48, the ratios agree quite well with the result from Fig. 3(c), with $mD_R/\rho D_T \approx 6$. For $\alpha = 2.20$, this ratio is about half the value of the other experiments; it is unclear why this is the case. To compare to the 3D result for spheres, we can use $A = \pi r^2$ to convert our ratio for the $\alpha = 1.00$ particle, leading to a value of $r^2_{\text{major}} D_R/D_T = 1.8$. For spheres diffusing in 3D, this ratio would be $3/4$ [28–30], so a somewhat similar order of magnitude. More generally, we have $A \equiv \pi r^2_{\text{major}}/\alpha$, so the ratio $\beta = r^2_{\text{major}} D_R/D_T = 1.8, 1.4, 1.5, 0.4$ for $\alpha = 1.00, 1.44, 1.48, 2.20$. This decreasing trend with increasing aspect ratio qualitatively disagrees with numerical results for 3D rod diffusion derived by Tirado and Garcia de la Torre [31,32]. For example, they found that when the aspect ratio of a rod is increased from 2 to 4, $\beta_4/\beta_2 = 1.4$, an increase. In contrast, when our aspect ratio is increased from 1.44 to 2.20, $\beta_{2.20}/\beta_{1.44} = 0.3$, a decrease. This disagreement suggests, not surprisingly, that the mechanism leading to diffusion in our 2D granular experiment are qualitatively different from normal 3D diffusion in liquids.

According to the classic Stokes-Einstein-Sutherland and Stokes-Einstein-Debye equations for D_T and D_R, respectively, the ratio D_T/D_R should be a constant independent of temperature and viscosity; the exact constant will depend on the diffusing particle shape. In glass-forming systems, prior observations found "decoupling" of translational and rotational diffusion, such that D_R/D_T is not constant but rather decreases as the glass transition is approached. This has been seen in experiments with small molecule glass-formers [33–35], colloidal glass experiments [11,12,36], and simulations [37–40]. Our bath particles appear a bit like they are approaching a glass transition as the magnetic forcing is decreased, as
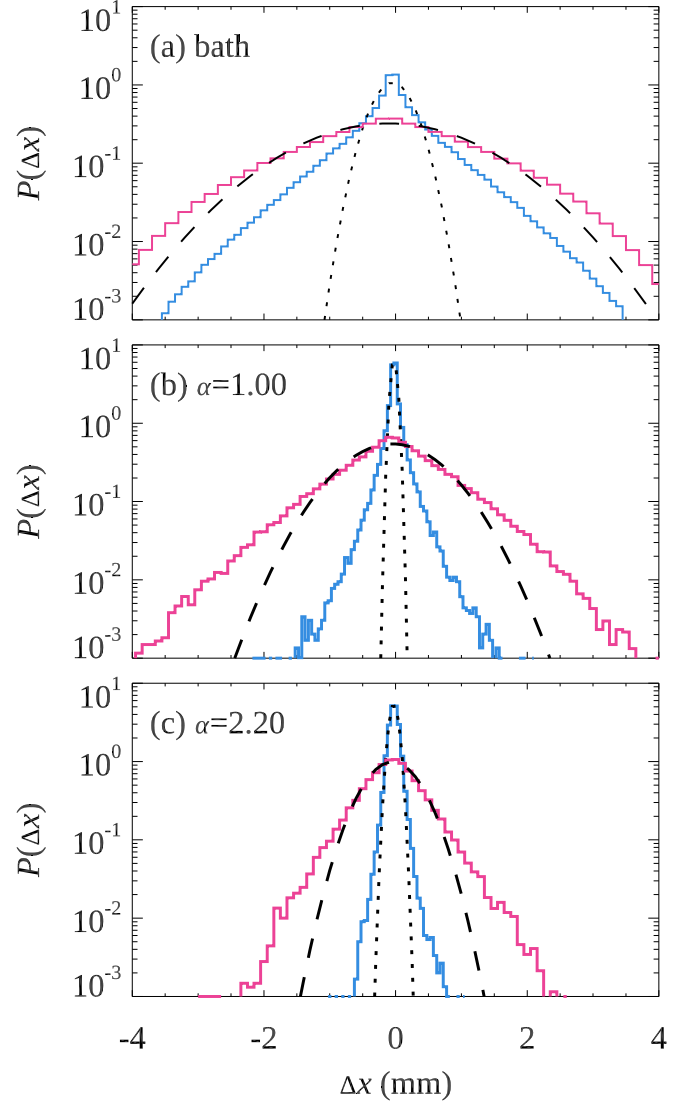

FIG. 9. Probability distribution functions $P(\Delta x)$ for (a) bath particles, (b) floating particles with aspect ratio $\alpha = 1.00$, and (c) floating particles with aspect ratio $\alpha = 2.20$. These are laboratory frame displacements, similar to the data shown in Fig. 5. In each case the blue data correspond to $L = 0.92$ mm (the lowest excitation) and the red data correspond to $L = 1.68$ mm (the highest excitation). $\Delta t = 0.1$ s is used to define the displacements. The dashed and dotted lines are Gaussian fits with the same standard deviation as the experimental data. The non-Gaussian parameter α_2 has the values (a) 1.1, 0.1; (b) 6.1, 0.5; (c) 2.3, 0.6 for small and large L.

seen by the subdiffusive behavior in Fig. 4 for the lowest forcing. Despite our bath particles becoming subdiffusive, in our experiments we do not observe decoupling of the translational and rotational diffusion: there is no systematic dependence of the data in Fig. 8. This is further evidence that the long-time behavior of the bath particles does not connect with the long-time behavior of the floating particles.

To better understand particle motion (both bath and floating particles), we show representative probability distribution functions of displacements in Fig. 9. In each panel the blue data are for the lowest excitation and are the narrow
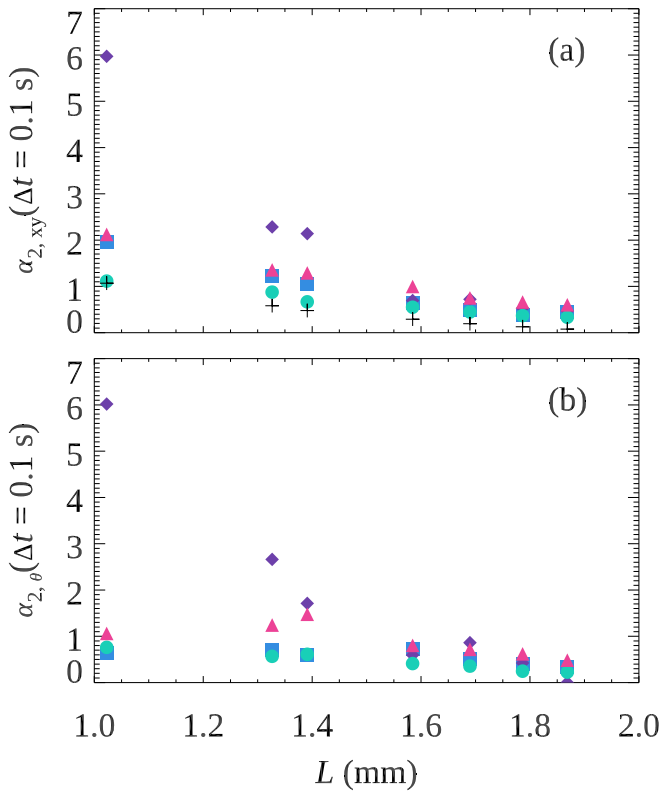
FIG. 10. (a) Non-Gaussian parameter for translational motion, evaluated at timescale $\Delta t = 0.1$ s. The symbols have the same meaning as in prior figures. The $+$ symbols are for the bath particles. (b) The same as in panel (a) but for rotational motion.

The relative width of the displacement probability distributions can be quantified with the non-Gaussian parameter $\alpha_2(\Delta t)$ [42],

$$\alpha_2(\Delta t) = \frac{\langle \Delta r^4 \rangle(\Delta t)}{2[\langle \Delta r^2 \rangle(\Delta t)]^2} - 1. \tag{1}$$

This quantity is zero for a Gaussian distribution, and positive for distributions with broad tails such as those shown in Fig. 9. The specific values of α_2 are given in the caption to the figure.

The non-Gaussian parameter is shown in Fig. 10(a) for translational motion and in Fig. 10(b) for rotational motion, as a function of the forcing strength L. For these results, the timescale $\Delta t = 0.1$ s is used to define displacements, although the qualitative behavior is not too sensitive to this choice. For low forcing, the non-Gaussian parameter is largest, reflecting the extreme width of the blue data in Fig. 9 as compared to the Gaussian fit. α_2 drops for larger L in Fig. 10. In this respect the behavior is similar to glassy liquids, which are more non-Gaussian close to the glass transition, and more Gaussian when in the liquid state [24,43,44].

IV. CONCLUSIONS

In our experiments the granular bath particles become subdiffusive at the lowest forcing L, while the floating particles are still diffusive. We conjecture this is because the floating particle does not interact with the bath particles directly. Typically one thinks of subdiffusive behavior in particle systems as arriving due to crowding of particles. In our experiment, no matter how the bath particles are crowded or interact with one another, the floating particle sits atop them and does not experience the crowding. It is interesting that the floating particle's long-time motion continues being diffusive even though the particles in the bath are not, and even though the floating particles' displacement probability distributions are non-Gaussian.

As described above, the bath particles are forced periodically with a period of 0.1 s, and this timescale appears to play a key role in determining the floating particle motion. It suggests that in our experiment we have a novel source of random energy acting like some sort of effective temperature. This may provide insight into other situations with nonthermal "effective temperature" baths.

distributions; the red data are for the highest excitation and are the broad distributions. The dotted and dashed black lines are Gaussian fits, and it is immediately apparent that the distributions are broader than a Gaussian. That is, large displacements are rare, but more common than would be expected if the distribution was a Gaussian of the same standard deviation. Non-Gaussian distributions are often seen in supercooled systems [24,25,41], so the result is plausible for the bath particles. It is intriguing that the distribution functions are non-Gaussian for the floating particles even though these particles are diffusive at long timescales (Fig. 6). That is, often strong non-Gaussian behavior is associated with a more pronounced plateau in the mean-square displacements; Fig. 6 shows a weak plateau, which is most obvious for the lowest forcing data. In all cases, the distributions are close to Gaussian for higher excitation. The same qualitative results are found for the rotational displacements (data not shown).

[1] K. Feitosa and N. Menon, Phys. Rev. Lett. **88**, 198301 (2002).

[2] R. P. Ojha, P. A. Lemieux, P. K. Dixon, A. J. Liu, and D. J. Durian, Nature **427**, 521 (2004).

[3] P. Melby *et al.*, J. Phys.: Condens. Matter **17**, S2689 (2005).

[4] J. G. Puckett and K. E. Daniels, Phys. Rev. Lett. **110**, 058001 (2013).

[5] C. Tapia-Ignacio, R. E. Moctezuma, and F. Donado, Phys. Rev. E **98**, 032901 (2018).

[6] G. W. Baxter and J. S. Olafsen, Nature **425**, 680 (2003).

[7] G. W. Baxter and J. S. Olafsen, Granul. Matter **9**, 135 (2007).

[8] F. Fujara, B. Geil, H. Sillescu, and G. Fleischer, Z. Phys. B **88**, 195 (1992).

[9] M. Lohfink and H. Sillescu, AIP Conf. Proc. **256**, 30 (1992).

[10] G. Biroli and J. P. Garrahan, J. Chem. Phys. **138**, 12A301 (2013).

[11] K. V. Edmond, M. T. Elsesser, G. L. Hunter, D. J. Pine, and E. R. Weeks, Proc. Nat. Acad. Sci. **109**, 17891 (2012).

[12] S. Vivek and E. R. Weeks, J. Chem. Phys. **147**, 134502 (2017).

[13] G. Marty and O. Dauchot, Phys. Rev. Lett. **94**, 015701 (2005).

[14] A. S. Keys, A. R. Abate, S. C. Glotzer, and D. J. Durian, Nat. Phys. **3**, 260 (2007).

[15] C. Xia *et al.*, Nat. Commun. **6**, 8409 (2015).

[16] K. E. Avila, H. E. Castillo, A. Fiege, K. Vollmayr-Lee, and A. Zippelius, Phys. Rev. Lett. **113**, 025701 (2014).

[17] K. E. Avila, H. E. Castillo, Vollmayr-Lee, and A. Zippelius, Soft Matter **12**, 5461 (2016).

[18] F. Donado, R. E. Moctezuma, L. López-Flores, M. Medina-Noyola, and J. L. Arauz-Lara, Sci. Rep. **7**, 12614 (2017).

[19] C. Tapia-Ignacio, J. Garcia-Serrano, and F. Donado, Phys. Rev. E **94**, 062902 (2016).

[20] R. E. Moctezuma, J. L. Arauz-Lara, and F. Donado, Physica A **496**, 27 (2018).

[21] F. Donado, J. M. Sausedo-Solorio, and R. E. Moctezuma, Phys. Rev. E **95**, 022601 (2017).

[22] I. F. Sbalzarini and P. Koumoutsakos, J. Struct. Biol. **151**, 182 (2005).

[23] J. P. Bouchaud and A. Georges, Phys. Rep. **195**, 127 (1990).

[24] W. Kob and H. C. Andersen, Phys. Rev. E **51**, 4626 (1995).

[25] G. L. Hunter and E. R. Weeks, Rep. Prog. Phys. **75**, 066501 (2012).

[26] P. M. Reis, R. A. Ingale, and M. D. Shattuck, Phys. Rev. Lett. **98**, 188301 (2007).

[27] L. López-Flores, H. Ruíz-Estrada, M. Chávez-Páez, and M. Medina-Noyola, Phys. Rev. E **88**, 042301 (2013).

[28] W. Sutherland, Phil. Mag. **9**, 781 (1905).

[29] A. Einstein, Ann. Phys. **322**, 549 (1905).

[30] P. Debye, *Polar Molecules* (Dover, Mineola, NY, 1929).

[31] M. M. Tirado and J. Garcia de la Torre, J. Chem. Phys. **71**, 2581 (1979).

[32] M. M. Tirado and J. Garcia de la Torre, J. Chem. Phys. **73**, 1986 (1980).

[33] F. H. Stillinger and J. A. Hodgdon, Phys. Rev. E **50**, 2064 (1994).

[34] I. Chang, F. Fujara, B. Geil, G. Heuberger, T. Mangel, and H. Sillescu, J. Non-Crystalline Solids **172-174**, 248 (1994).

[35] M. T. Cicerone and M. D. Ediger, J. Chem. Phys. **104**, 7210 (1996).

[36] G. H. Koenderink, H. Zhang, D. G. A. L. Aarts, M. P. Lettinga, A. P. Philipse, and G. Nägele, Faraday Discuss. **123**, 335 (2003).

[37] M. G. Mazza, N. Giovambattista, F. W. Starr, and H. E. Stanley, Phys. Rev. Lett. **96**, 057803 (2006).

[38] S. H. Chong, A. J. Moreno, F. Sciortino, and W. Kob, Phys. Rev. Lett. **94**, 215701 (2005).

[39] S. H. Chong and W. Kob, Phys. Rev. Lett. **102**, 025702 (2009).

[40] S. K. Kumar, G. Szamel, and J. F. Douglas, J. Chem. Phys. **124**, 214501 (2006).

[41] J. S. Olafsen and J. S. Urbach, Phys. Rev. E **60**, R2468(R) (1999).

[42] A. Rahman, Phys. Rev. **136**, A405 (1964).

[43] W. Kob, C. Donati, S. J. Plimpton, P. H. Poole, and S. C. Glotzer, Phys. Rev. Lett. **79**, 2827 (1997).

[44] M. S. Shell, P. G. Debenedetti, and F. H. Stillinger, J. Phys.: Condens. Matter **17**, S4035 (2005).